Long-lived magnons throughout the Brillouin zone of the strong-leg spin ladder $(C_7H_{10}N)_2CuBr_4$

D. Schmidiger,* S. Mühlbauer, S. N. Gvasaliya, T. Yankova,† and A. Zheludev‡
Neutron Scattering and Magnetism, Institute for Solid State Physics, ETH Zurich, Switzerland
(Received 24 May 2011; revised manuscript received 3 August 2011; published 18 October 2011)

Inelastic neutron scattering is used to measure spin excitations in fully deuterated single-crystal samples of the strong-leg antiferromagnetic $S = 1/2$ spin ladder compound $(C_7D_{10}N)_2CuBr_4$. Sharp resolution-limited magnons are observed across the entire one-dimensional Brillouin zone. The results validate the previously proposed symmetric spin ladder model and provide a reliable estimate of the relevant exchange interactions.

DOI: 10.1103/PhysRevB.84.144421 PACS number(s): 75.10.Jm, 75.10.Kt, 75.40.Gb

I. INTRODUCTION

The $S = 1/2$ Heisenberg antiferromagnetic (AF) spin ladder is arguably the most important model in quantum magnetism. Of particular interest are spin ladders with dominant leg interactions. They are properly described as a pair of weakly coupled spin chains. Correspondingly, the gapped magnons ($S = 1$ excitations) are bound states of spinons propagating on the legs.[1] This is in contrast to strong-rung ladders,[2–5] where excitations are better described in terms singlet-triplet transitions in weakly interacting AF dimers on the ladder rungs.[6–8] Until very recently, the only known strong-leg spin ladder systems were $Sr_{14}Cu_{24}O_{41}$ and its derivatives, where the magnetic excitation spectrum was studied by inelastic neutron[9,10] and resonant x-ray scattering[11] techniques. Unfortunately, the energy scale in these materials is too large to make it useful for systematic studies of the many interesting quantum phenomena predicted to occur in external magnetic fields or at finite temperatures.

An almost perfect realization of a strong-leg ladder model was recently found in the organometallic compound $(C_7H_{10}N)_2CuBr_4$, DIMPY for short.[12,13] It is characterized by a rather low energy scale, particularly the energy gap $\Delta = 0.32$ meV, and the excellent one-dimensionality. These features enabled a direct observation of a spin liquid to Luttinger spin liquid quantum phase transition in applied magnetic fields in this material.[13] Inelastic neutron scattering experiments were also performed, and the magnon dispersion relation was measured in the vicinity of the AF zone center. This information was then used to estimate the ratio of Heisenberg exchange constants for the ladder legs and rungs, respectively: $J_{\rm leg}/J_{\rm rung} \sim 2.2$.[13] Unfortunately, the dispersion near the zone center is not very sensitive to this parameter and does not allow to unambiguously establish the spin Hamiltonian. Measurements in the remaining 2/3 of the Brillouin zone were inhibited by the use of only partially deuterated single-crystal samples, as hydrogen scattering is a huge contributor to neutron background. In the present study we used fully deuterated DIMPY single-crystal samples to measure the single-magnon excitation spectrum across the entire Brillouin zone.

The crystal structure of DIMPY was described in Ref. 12. The material is monoclinic, space group $P2_1/n$, with room-temperature lattice parameters $a = 7.50$ Å, $b = 31.61$ Å, $c = 8.20$ Å, and $\beta = 98.97^\circ$.[12] As schematically shown in Fig. 1, the key structural features are ladders that run along the crystallographic a direction and are composed of magnetic Cu^{2+} ions, bridged by robust Cu-Br-Br-Cu covalent superexchange pathways. The organic ligands provide spacing between such ladders and ensure an almost perfect magnetic one-dimensionality. There are two types of ladders in the crystal structure, related by symmetry and described by the rung vectors $\mathbf{d}_{1,2} = (0.423, \pm 0.256, 0.293)$ in fractional coordinates. The existence of two different ladder systems was not explicitly discussed in Refs. 12 and 13. Nevertheless, the ladder systems are visible in Fig. 2(b) of Ref. 12. In projection onto the (a,c) plane these become equivalent. This is a crucial circumstance, since it allows to independently measure the leg-odd and leg-even spin excitation spectra in this compound. The total spin-dynamic structure factor for a symmetric ladder can be decomposed into its even and odd parts[14]:

$$2\mathcal{S}(\mathbf{q},\omega) = \mathcal{S}^+(\mathbf{q},\omega)\,[1 + \cos(\mathbf{q}\cdot\mathbf{d})] + \mathcal{S}^-(\mathbf{q},\omega)\,[1 - \cos(\mathbf{q}\cdot\mathbf{d})]\,. \quad (1)$$

Here, $\mathbf{d}$ defines the ladder rung, and $\mathcal{S}^+(\mathbf{q},\omega)$ and $\mathcal{S}^-(\mathbf{q},\omega)$ are structure factors written for the sum (even) and difference (odd) of spins on each rung. The significance of this decomposition is that the single-magnon excitations are contained in the odd channel, while the lowest-energy leg-even excitations are a two-magnon continuum.[14] In reciprocal space, the scattering due to the two channels is well separated thanks to the phase factors in Eq. (2). This separation has been previously made use of in the study of $Sr_{14}Cu_{24}O_{41}$ (Ref. 10) and other systems. For the particular case of DIMPY, it is enabled for a scattering vector $\mathbf{q}$ in the $(h,0,l)$ plane, where the product $(\mathbf{q}\cdot\mathbf{d})$ is the same for the two symmetry-related ladders. The corresponding phase factor for the odd channel is plotted in Fig. 2. In our experiments, following Ref. 13, we focused on the $(h,0,1.7 - 1.44h)$ reciprocal-space rod, where only the leg-odd correlations are observed and the single-magnon scattering intensity is maximized. In the presence of any asymmetry of the spin Hamiltonian with respect to an interchange of ladder legs, Eq. (2) will no longer hold. For DIMPY, simple symmetric nearest-neighbor leg and rung exchange interactions are expected to dominate due to structural considerations. As a result, the Hamiltonian asymmetry is negligible. As will be discussed below, this fact is further supported by our measurements of the magnon dispersion.

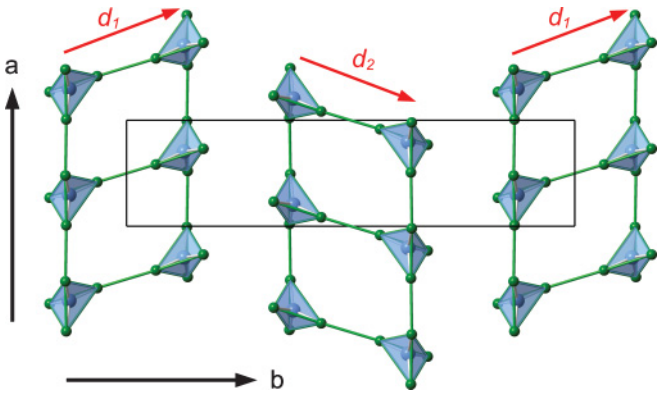

FIG. 1. (Color online) A schematic representation of the antiferromagnetic spin ladders in $(C_7D_{10}N)_2CuBr_4$ in projection onto the (a,b) crystallographic plane. $S = 1/2$ carrying Cu^{2+} ions (blue) are connected by double Br^- (green) bridges. The vectors $\mathbf{d}_{1,2}$ define the rung of the ladders. The solid black line indicates the unit cell. The organic ligand plays no role in the magnetism and is not shown.

II. EXPERIMENTAL SETUP

For the present experiment, five fully deuterated single crystals were grown from solution by slow diffusion in a temperature gradient. Inelastic neutron scattering experiments were performed with a single crystal ($m = 700$ mg) as well as with four crystals ($m = 3.7$ g) which were coaligned to a final mosaic spread of better than 1.5°. The measurements were performed on the TASP cold-neutron triple axis spectrometer[15] installed at the SINQ spallation source at Paul Scherrer Institut and operated by ETH, Zürich. Pyrolytic graphite monochromator and horizontally focusing analyzer were used in combination with a Be filter after the sample. Most of the data were collected in constant-q scans with $E_f = 3.5$ meV fixed-final-energy neutrons. The sample environment was a ^{3}He-^{4}He dilution refrigerator: all scans were performed at $T = 100$ mK.

III. RESULTS AND DISCUSSION

Typical raw scans are plotted in symbols in Fig. 3. In the entire Brillouin zone, the magnon excitations are clearly visible as well defined inelastic peaks, on a mostly flat background of approximately 5 counts/min. The latter was shown to be of nonmagnetic origin by comparing the background to scans performed at $T = 80$ and 160 K. It primarily originates from the sample itself. The bulk of the data is shown in the false-color plot in Fig. 4. Since experiments were performed with two different samples, the data can not be combined to a single color plot. Data measured with four coaligned crystals for $0.5 < h < 1$ are shown as a false-color plot only.

The data were analyzed using a parameterized cross-section function, written in the single mode approximation (SMA),

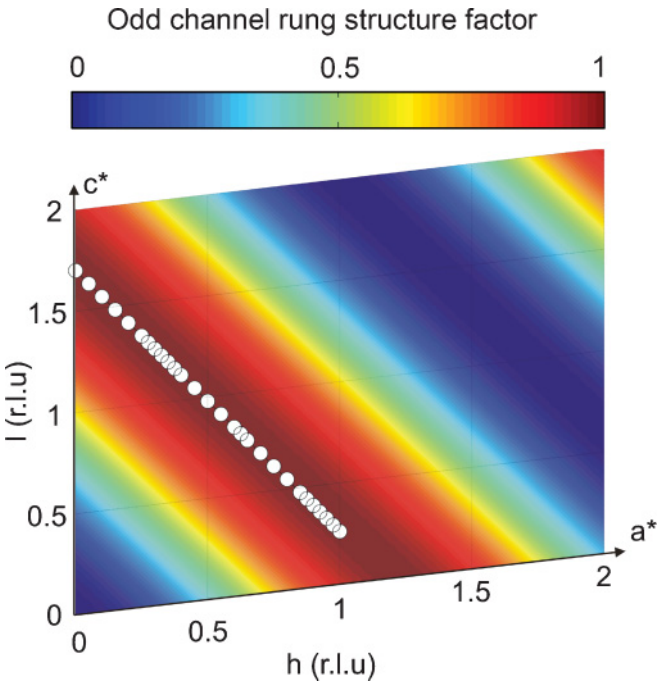

FIG. 2. (Color online) False-color plot of the antiferromagnetic rung structure factor for $(C_7D_{10}N)_2CuBr_4$ (DIMPY) for momentum transfers in the $(h,0,l)$ reciprocal-space plane. The color mapping ranges from zero (dark blue), through green and yellow, to the maximum value (red). White circle symbols represent the wave vectors of all measured inelastic neutron scans, along the $(h,0,1.7-1.44h)$ line, as in Ref. 13. The ladders are aligned along the crystallographic a axis, i.e., perpendicular to c^*.

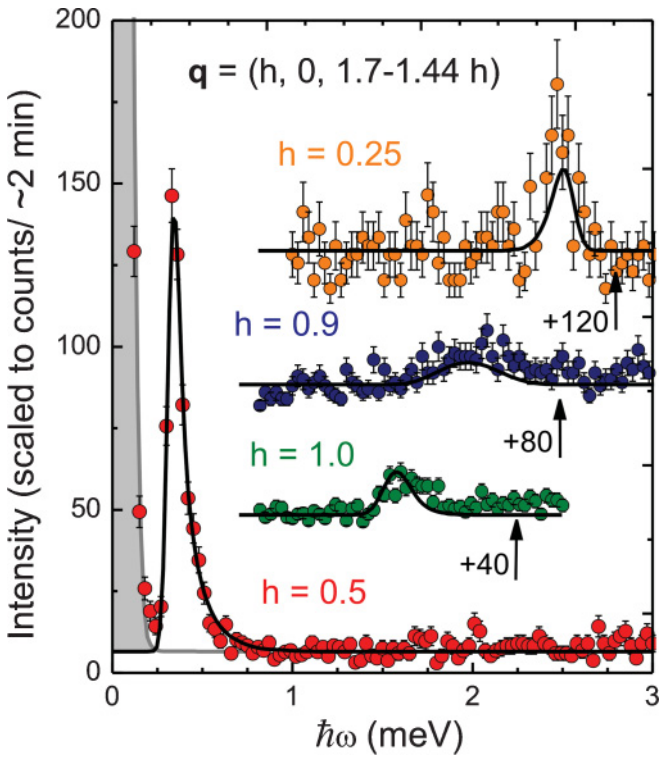

FIG. 3. (Color online) Symbols: typical inelastic neutron scattering scans collected in $(C_7D_{10}N)_2CuBr_4$ at the one-dimensional antiferromagnetic zone center, ferromagnetic zone center, and near the antiferromagnetic zone boundary. The solid lines represent a *simultaneous* fit of Eqs. (2)–(4) to 29 constant-q scans, as described in the text. The gray area is the estimated elastic incoherent background.

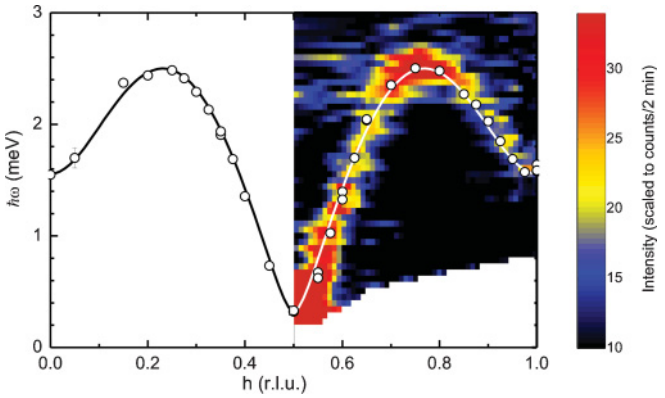

FIG. 4. (Color online) Dispersion of magnons measured in $(C_7D_{10}N)_2CuBr_4$ for wave vectors along the $(h,0,1.7-1.44h)$ reciprocal-space rod. Symbols: excitation energies as determined in fits to individual scans. Solid line: equation (3) with parameters obtained in a simultaneous fit to 29 constant-q scans. False-color overlay: the bulk of experimental data at $h > 0.5$.

with the empirical dispersion relation[14] previously also used for IPA-$CuCl_3$[3]:

$$\mathcal{S}(\mathbf{q},\omega) \propto \mathcal{S}(\mathbf{q})\delta(\omega - \omega_{\mathbf{q}}), \tag{2}$$

$$(\hbar\omega_{\mathbf{q}})^2 = \Delta^2 \sin^2(\pi h) + A^2 \cos^2(\pi h) + B^2 \sin^2(2\pi h). \tag{3}$$

Here, $\mathbf{q} = h\mathbf{a}^* + k\mathbf{b}^* + l\mathbf{c}^*$, Δ, A, and B parametrize the dispersion relation, respectively. Assuming the SMA accounts for most of the inelastic scattering in the leg-odd channel, and that only nearest-neighbor leg and rung interactions are relevant, the equal-time structure factor is obtained from the Hohenberg-Brinkman first-moment sum rule[16,17]:

$$\hbar\omega_{\mathbf{q}}\mathcal{S}(\mathbf{q}) \propto -\tfrac{4}{3}E_{\text{leg}}[1-\cos\mathbf{q}\cdot\mathbf{a})]-\tfrac{2}{3}E_{\text{rung}}[1-\cos(\mathbf{q}\cdot\mathbf{d})]. \tag{4}$$

In this formula, $E_{\text{rung}} = J_{\text{rung}}\langle\mathbf{S}_1\mathbf{S}_2\rangle$ is the mean exchange energy on the ladder rung and E_{leg} is defined similarly. For all our data $\mathbf{q}\cdot\mathbf{d} = \pi$, so the second term in the RHS is reduced to a constant.

The cross section was numerically convoluted[18] with the spectrometer resolution function calculated in the Popovici approximation[19] and *globally* fit to the bulk of available experimental data (29 constant-q scans). The magnetic form factor for Cu^{2+} ions was built into the fits. In the analysis, we assumed a background consisting of a flat component and a resolution-limited Gaussian peak at zero energy transfer, the latter to account for elastic incoherent scattering. Scans collected at $0.65 < h < 0.8$ with $E_f = 3.5$ meV were excluded from the global fit due to an apparent nondispersive feature in the background at around 2.1 meV energy transfer at these wave vectors. The latter was independently verified to be of nonmagnetic origin (by collecting background data at 80 and 160 K), and shown not to affect the data measured at equivalent wave vectors in the other half of the Brillouin zone. The least-squares global fitting procedure yields good agreement with $\Delta = 0.33(1)$ meV, $A = 1.55(1)$ meV, $B = 2.27(1)$ meV, and $E_{\text{leg}}/E_{\text{rung}} = 1.42(16)$ with $\chi^2 = 3.1$. The relatively large χ^2 value is not surprising, since the slight q dependence of the

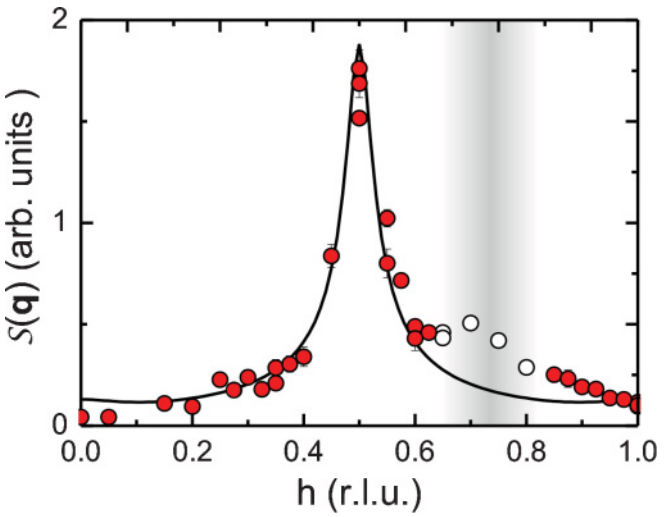

FIG. 5. (Color online) Symbols: equal-time spin structure factor $\mathcal{S}(\mathbf{q})$, as determined in fits to individual scans. The shaded area and open symbols show scans excluded from the global fit due to a possible background contamination of nonmagnetic origin. Solid line: equation (4), with parameters obtained in the global fit.

nondispersive features in the background was not taken into account by the global fitting model. Scans simulated using these parameter values are shown as solid lines in Fig. 3. The resulting dispersion relation and equal-time structure factor are plotted in Figs. 4 and 5, respectively. Symbols in the two latter figures were obtained in intensity and central energy fits to individual scans, as opposed to global fits to all the measured data. Typical individual scans yielded a chi-square value of $\chi^2 = 1.4$. Any remaining discrepancies, especially in what concerns excitation intensity, may be attributed to neutron absorbtion in the sample. This effect could not be taken into account due to the irregular sample shape. In conclusion, the SMA description of the magnon excitation is in good agreement with both the dispersion and the intensity of the neutron data.

The measured magnon spectrum in DIMPY is markedly different from the one previously seen in IPA-$CuCl_3$,[3,20] even though the dispersion relation is similar. In the latter material, the single-magnon branch was found to terminate at some critical wave vector before reaching the ferromagnetic zone center. This effect was attributed to a two-magnon decay.[3,21] It is now understood that in one dimension, this process, if only allowed by symmetry, will always render the sharp single-magnon excitation unstable in the $\hbar\omega - \mathbf{q}$ region spanned by two-particle momenta and energies.[22] As was previously done for IPA-$CuCl_3$,[3] knowing the single-particle dispersion relation allows us to estimate the boundaries of this magnon-exclusion region for DIMPY: $-\xi_c + n < \mathbf{q}\cdot\mathbf{a}/(2\pi) < \xi_c + n$, where n is integer and $\xi_c \sim 0.85$. Experimentally, no anomalies in the magnon branch are observed at the critical wave vectors $n \pm \xi_c$. The magnon branch persists in the entire Brillouin zone and to within experimental error remains resolution-limited. This implies that single-magnon states are protected from two-magnon decay by symmetry. The relevant symmetry operation is an interchange of the two ladder legs. Indeed, as mentioned in the introduction, magnons are leg-odd excitations, while two-magnon states are leg-even. Thus the

stability of magnons in DIMPY validates the symmetric-ladder model for this compound. In contrast, in IPA-$CuCl_3$, symmetry-breaking interactions along the ladder diagonal are known to be significant.[4]

Using the measured dispersion relation and the numerical results of Ref. 13 we can estimate $J_{\rm leg}/J_{\rm rung} \sim 2.0$. The dominance of the leg exchange coupling is also manifested in the experimental ratio $E_{\rm leg}/E_{\rm rung} \sim 1.4$, independently determined from excitation intensities. However, this latter estimate should be treated with a degree of caution, as it relies on the SMA. This approximation is obviously not exact. Specifically, it does not allow for any continuum excitations, which actually becomes progressively more important as the relative rung strength decreases.

In summary, our measurements confirm that DIMPY is perhaps the most "perfect" known spin ladder material, with dominant leg interactions, stable magnons across the entire Brillouin zone and experimentally accessible energy scales. The obvious next step will be to study multimagnon continua and the evolution of the excitation spectrum in high magnetic fields.

ACKNOWLEDGMENTS

This work is partially supported by the Swiss National Fund under project 2-77060-11 and through Project 6 of MANEP. The neutron experiments would be impossible without expert technical support provided by Paul Scherrer Institut, particularly by Markus Zolliker and the sample environment team. We thank V. Glazkov (Kapitza Institute, Russian Academy of Science) for his involvement at the early stages of this project.

---

*This work is part of the Masters thesis project of David Schmidiger.
†Permanent address: Chemistry Dept., Moscow State University, Moscow, Russia.
‡zhelud@ethz.ch

[1] D. G. Shelton, A. A. Nersesyan, and A. M. Tsvelik, Phys. Rev. B **53**, 8521 (1996).
[2] B. C. Watson, V. N. Kotov, M. W. Meisel, D. W. Hall, G. E. Granroth, W. T. Montfrooij, S. E. Nagler, D. A. Jensen, R. Backov, M. A. Petruska, G. E. Fanucci, and D. R. Talham, Phys. Rev. Lett. **86**, 5168 (2001).
[3] T. Masuda, A. Zheludev, H. Manaka, L.-P. Regnault, J.-H. Chung, and Y. Qiu, Phys. Rev. Lett. **96**, 047210 (2006).
[4] T. Fischer, S. Duffe, and G. S. Uhrig, e-print arXiv:1009.3375v2 (unpublished).
[5] A. T. Savici, G. E. Granroth, C. L. Broholm, D. M. Pajerowski, C. M. Brown, D. R. Talham, M. W. Meisel, K. P. Schmidt, G. S. Uhrig, and S. E. Nagler, Phys. Rev. B **80**, 094411 (2009).
[6] A. K. Kolezhuk and H.-J. Mikeska, Int. J. Mod. Phys. B **12**, 2325 (1998).
[7] V. N. Kotov, O. P. Sushkov, and R. Eder, Phys. Rev. B **59**, 6266 (1999).
[8] B. Normand and Ch. Rüegg, Phys. Rev. B **83**, 054415 (2011).
[9] R. S. Eccleston, M. Uehara, J. Akimitsu, H. Eisaki, N. Motoyama, and S. I. Uchida, Phys. Rev. Lett. **81**, 1702 (1998).
[10] S. Notbohm, P. Ribeiro, B. Lake, D. A. Tennant, K. P. Schmidt, G. S. Uhrig, C. Hess, R. Klingeler, G. Behr, B. Büchner, M. Reehuis, R. I. Bewley, C. D. Frost, P. Manuel, and R. S. Eccleston, Phys. Rev. Lett. **98**, 027403 (2007).
[11] J. Schlappa, T. Schmitt, F. Vernay, V. N. Strocov, V. Ilakovac, B. Thielemann, H. M. Rønnow, S. Vanishri, A. Piazzalunga, X. Wang, L. Braicovich, G. Ghiringhelli, C. Marin, J. Mesot, B. Delley, and L. Patthey, Phys. Rev. Lett. **103**, 047401 (2009).
[12] A. Shapiro, C. P. Landee, M. M. Turnbull, J. Jornet, M. Deumal, J. J. Novoa, M. A. Robb, and W. Lewis, J. Am. Chem. Soc. **129**, 952 (2007).
[13] T. Hong, Y. H. Kim, C. Hotta, Y. Takano, G. Tremelling, M. M. Turnbull, C. P. Landee, H.-J. Kang, N. B. Christensen, K. Lefmann, K. P. Schmidt, G. S. Uhrig, and C. Broholm, Phys. Rev. Lett. **105**, 137207 (2010).
[14] T. Barnes and J. Riera, Phys. Rev. B **50**, 6817 (1994).
[15] F. Semadeni, B. Rössli, and P. Böni, Physica B **297**, 152 (2001).
[16] P. C. Hohenberg and W. F. Brinkman, Phys. Rev. B **10**, 128 (1974).
[17] I. Zaliznyak and S.-H. Lee, *Modern Techniques of Characterizing Magnetic Materials* (Kluwer Academic, Boston, Dordrecht, London, 2005), Chap. 1.3.6.2, p. 41.
[18] A. Zheludev, *Reslib Resolution Library for* MATLAB, [http://www.neutron.ethz.ch/research/resources/reslib] (2009).
[19] M. Popovici, Acta Crystallogr. Sect. A **31**, 507 (1975).
[20] A. Zheludev, V. O. Garlea, T. Masuda, H. Manaka, L.-P. Regnault, E. Ressouche, B. Grenier, J.-H. Chung, Y. Qiu, K. Habicht, K. Kiefer, and M. Boehm, Phys. Rev. B **76**, 054450 (2007).
[21] M. B. Stone, I. A. Zaliznyak, T. Hong, C. L. Broholm, and D. H. Reich, Nature (London) **440**, 190 (2006).
[22] M. E. Zhitomirsky, Phys. Rev. B **73**, 100404 (2006).